

IC10 单晶过渡液相扩散焊接头微观组织与力学性能

郎 波, 侯金保, 吴 松

(北京航空制造工程研究所 航空发动机工艺研究室, 北京 100024)

摘 要: 采用扫描电镜(SEM)和能谱分析仪(EDS)研究 IC10 单晶高温合金过渡液相(TLP)扩散焊接头微观组织演变。结果表明, 接头由连接区和基体区所组成, 连接区由等温凝固区和快速凝固区组成。快速凝固区可以通过延长保温时间的方法予以消除。随着保温时间从 2 h 增加到 8 h, 基体内的 γ' 相尺寸达到了 $0.9 \mu\text{m}$ 。通过限制 TLP 扩散焊接头内晶界的形成, 以及焊后固溶处理的方法可以有效提高接头的力学性能。在温度 $1\ 000\ ^\circ\text{C}$ 下, 接头平均抗拉强度为 $507\ \text{MPa}$ 。在温度 $1\ 000\ ^\circ\text{C}$ 、应力 $144\ \text{MPa}$ 下接头持久寿命可达到 120 h 以上。

关键词: IC10 单晶; TLP 扩散焊; 微观组织

中图分类号: TG453 文献标识码: A 文章编号: 0253-360X(2012)08-0109-04



郎 波

0 序 言

随着航空发动机推重比和涡轮前温度的不断提高, 以及涡轮级数不断减少, 单级负荷不断增大, 涡轮叶片的应力水平越来越高, 工况越趋恶劣, 必须寻求更可靠、更先进的材料、工艺和结构才能满足未来高性能发动机的设计要求。单晶高温合金具有优良的高温蠕变和疲劳性能, 已成为国际上制造先进航空发动机涡轮叶片的首选材料。因此开发出能实现单晶高温合金可靠、高性能连接的先进焊接技术, 对单晶合金的工程推广应用具有重要的现实意义。

采用熔化焊和钎焊焊接单晶高温合金时满足不了单晶生长的要求, 焊接接头无法形成单晶化组织, 从而显著降低接头的力学性能。扩散焊可用于单晶高温合金的连接, 但是这种方法需要采用较大的压力, 配合面精度要求高, 对于复杂构件很难均匀加压, 甚至还需要昂贵和复杂的夹具。过渡液相(transient liquid phase, TLP)扩散焊结合了钎焊和扩散焊二者的技术优点, 能获得组织与成分均匀的高性能接头, 已成为定向凝固合金、氧化物弥散强化合金等新材料的首选连接方法^[1,2], 其可以实现单晶高温合金的优质连接, 避免在连接区产生大角度的晶界^[3-6]。

国内对单晶材料 TLP 扩散连接机理的研究还不够深入, 现有技术无法满足高推比航空发动机研制的需要。文中针对高性能航空发动机涡轮叶片研

制所需的 IC10 单晶, 开展 TLP 扩散焊技术研究, 旨在揭示 IC10 单晶 TLP 扩散焊接头微观组织特点及其与力学性能的关系。

1 试验方法

试验用材料为 [001] 取向的 $\phi 15\ \text{mm}$ 棒状 IC10 单晶高温合金, 其在温度 $1\ 000\ ^\circ\text{C}$ 、保温时间 100 h 条件下持久强度为 $160\ \text{MPa}$, 其成分为 Ni59.9, Cr6.9, Al5.7, Co12.2, Mo1.8, W4.9, Hf1.5, Ta7.1 (质量分数, %)。微观组织主要由网状 γ 和 γ' 相组成, 其中树枝状的 γ 相为基体, 立方体状的 γ' 为沉淀析出相, 如图 1 所示。将 IC10 单晶加工成 $\phi 15\ \text{mm} \times 4\ \text{mm}$ 和 $\phi 15\ \text{mm} \times 36\ \text{mm}$ 的试样, 分别用于 TLP 扩散焊接头微观组织分析与力学性能测试。TLP 扩散焊采用以 IC10 单晶为基体加入 2%~3% (质量分数) 的 B 元素作为降熔元素的粉末状中间

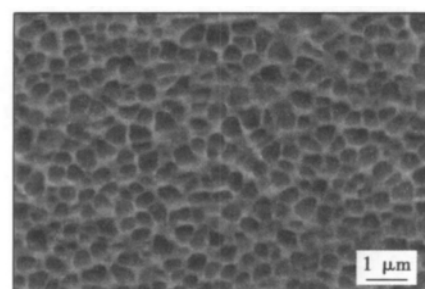


图 1 IC10 单晶高温合金微观组织形貌

Fig. 1 Microstructure of IC10 single crystal superalloy

层,而焊接间隙约为 $40\ \mu\text{m}$.

待焊 IC10 单晶试样需要严格配对加工,采用 VBF-80 型真空钎焊炉进行 TLP 扩散焊试验. 焊接之后,垂直于焊接面方向将接头剖开作为金相试样. 其横截面经过打磨、抛光后,再采用化学腐蚀方法对接头进行腐蚀,腐蚀剂为 $\text{CuSO}_4(20\ \text{g}) + \text{浓 HCl}(80\ \text{mL}) + \text{H}_2\text{O}(100\ \text{mL})$,利用扫描电镜(SEM)和能谱分析仪(EDS)对 TLP 扩散焊接头进行微观组织及成分分析.

2 试验结果与分析

2.1 接头微观组织特点

图2为焊接温度 $1\ 240\ ^\circ\text{C}$ 、保温时间 2 h 条件下接头微观组织形貌. 结果表明,接头由连接区(A)和基体区(B)所组成,未发现明显的扩散区特征. SEM 观察发现连接区由等温凝固区和快速凝固区组成,如图3所示. 等温凝固区是在中间层熔化后的保温过程中形成的. 保温过程中,液态中间层中的降熔元素向基体扩散而使中间层内的降熔元素浓度减小,进而提高了液态中间层的熔点,当中间层熔点高于焊接温度时,将发生等温凝固过程. 而等温凝固区主要由 γ 和 γ' 相组成. 如果在保温过程中接头未实现完全的等温凝固,那么在随后的冷却过程中,接头内的残余液相将凝固而形成快速凝固区. C 区的 EDS 分析结果为 Ni5.82, Mo27.17, W39.80, Cr21.78, Co3.75, Ti1.37, Mn0.31(质量分数, %), 由此可知, C 区为 (Mo, W, Cr) B 的化合物. 根据接头微观组织形貌可知,快速凝固区主要是由花簇状的 γ 和 γ' 相共晶及 γ 相和 (Mo, W, Cr) B 化合物共晶组织组成.

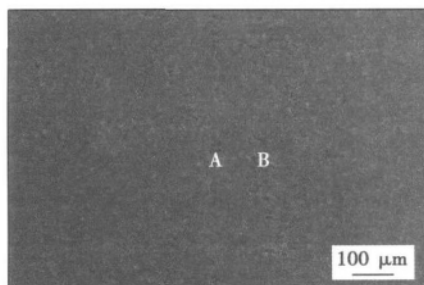


图2 在温度 $1\ 240\ ^\circ\text{C}$ 下保温时间 2 h 接头微观组织形貌
Fig. 2 Optical morphology of joint under conditions of $1\ 240\ ^\circ\text{C}$ temperature and 2 h time

在焊接温度 $1\ 240\ ^\circ\text{C}$ 下,分别保温 4, 6, 8 h 时,接头微观组织形貌如图4所示. 结果表明,随着焊

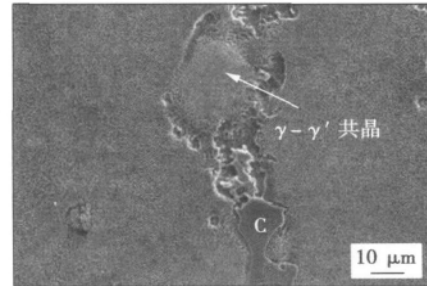
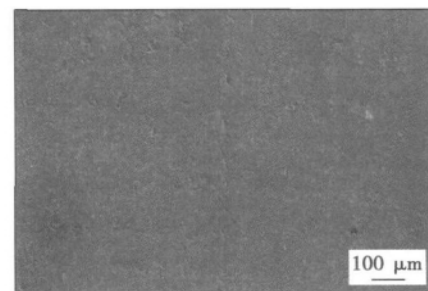
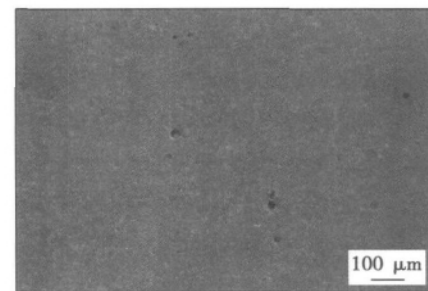


图3 接头高倍下形貌
Fig. 3 Morphology of joint at relatively high magnification

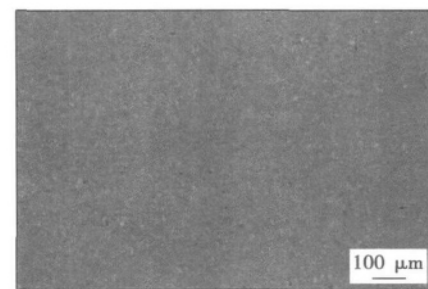
接时间的增加,接头内快速凝固区的宽度逐渐减小,等温凝固区宽度逐渐增大. 当焊接时间为 2, 4 h 时,快速凝固区连续分布在接头中心线上,其由 (Mo, W, Cr) B 化合物和 γ 相共晶及 γ 和 γ' 相共晶组织组



(a) 保温时间为 4 h



(b) 保温时间为 6 h

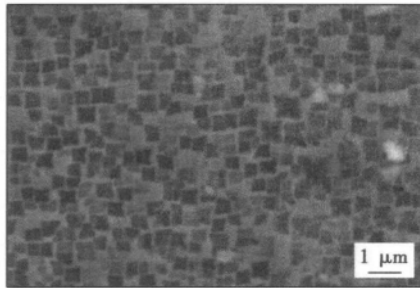


(c) 保温时间为 8 h

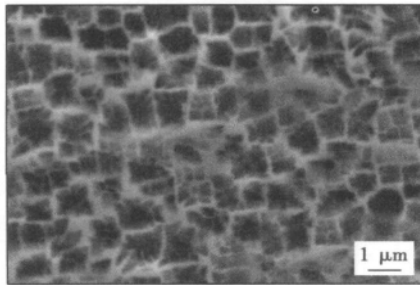
图4 在温度 $1\ 240\ ^\circ\text{C}$ 下保温时间对接头微观组织的影响
Fig. 4 Effect of welding time on joint optical morphology under condition of $1\ 240\ ^\circ\text{C}$ welding temperature

成;当焊接时间为6 h时,由于焊缝间隙的不一致性使快速凝固区呈不连续分布,其相组成与焊接时间为2.4 h时相同;当焊接时间达到8 h时,快速凝固区消失,等温凝固已经完成.因此可以通过适当延长焊接时间而使液态中间层内B元素充分扩散的方式来消除接头中心的快速凝固区.

图5给出了保温时间对基体微观组织形貌的影响.可以看出,在温度1240℃下保温时间为2 h时,基体内的 γ' 相呈立方体状,且立方度较高,平均边长约为0.4 μm .随着保温时间的延长,基体内的立方体状 γ' 相平均边长增加,且棱角发生钝化.当保温时间增加到8 h时, γ' 相平均边长增加到0.9 μm ,且棱角钝化严重,逐渐向球形发展.



(a) 保温时间为2 h



(b) 保温时间为8 h

图5 在温度1240℃下保温时间对基体微观组织的影响
Fig. 5 Effect of welding time on microstructure of parent material under condition of 1240℃ welding temperature

单晶高温合金中 γ' 相的形貌与 γ/γ' 两相错配度密切相关.当保温时间较短时, γ' 相发生长大,从而增加了 γ/γ' 两相的错配度,但 γ 和 γ' 两相仍然保持共格关系, γ' 相的形貌主要取决于应变能的作用,而立方体形态具有最小的应变能,为降低应变能, γ' 长大并且呈规则的立方体形状.当保温时间延长时, γ' 相继续长大, γ/γ' 两相错配度增加,从而超越了弹性范围, γ/γ' 两相不能保持共格关系,在两相界面上产生错配位错,而使应变能降低,因此界面能起

主要作用, γ' 相的形貌将趋于圆形而使 γ' 相棱角发生钝化.

2.2 接头微观组织与力学性能的关系

IC10单晶高温合金的固溶处理温度是1260℃,为了避免TLP扩散焊接头内形成大角度晶界及发生溶蚀现象,获得TLP扩散焊与固溶处理的一体化工艺,在保证两单晶取向差在合适范围内的条件下,采用在1200℃温度下保温9 h,然后在1260℃温度下保温2 h的工艺进行TLP扩散焊试验,焊后充氩气进行冷却,基体微观组织如图6所示.结果表明,基体内的 γ' 相呈立方体状,且立方度较高,平均边长约为0.4 μm .这主要是由于工艺中加入了固溶处理过程,因此在固溶处理后快速冷却过程中将析出细小、均匀分布的 γ' 相粒子,随着温度的降低, γ' 相发生长大而呈立方体状.此外,IC10单晶经过此工艺的热处理后,在温度1000℃下的平均抗拉强度达到555 MPa,其断口形貌如图7所示.结果表明,断口具有明显的延性断裂特征, γ' 基体相表现为韧性撕裂特征.

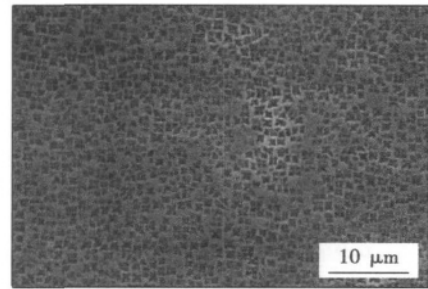


图6 TLP扩散焊后基体微观组织形貌
Fig. 6 Microstructure of parent material after TLP diffusion bonding

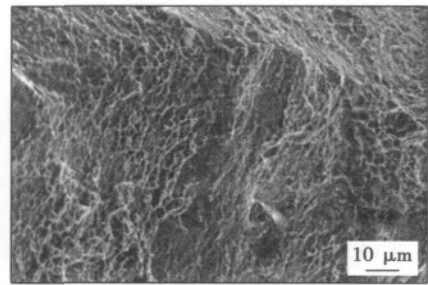


图7 IC10单晶高温拉伸断口形貌
Fig. 7 Morphology of IC10 single crystal superalloy fracture surface after tensile test under high temperature

在温度1200℃下保温9 h,然后在温度1260℃下保温2 h的条件下,TLP扩散焊接头微观组织

形貌如图8所示。结果表明,连接区内有硼化物存在。高倍下可以看出,连接区微观组织与基体区微观组织相近(图9)。连接区组织特征是立方 γ' 相以共格方式镶嵌在 γ 基体中, γ' 相的立方度较高,且形状规则,立方 γ' 的平均边长约为 $0.4\ \mu\text{m}$,连接区内未发现有明显的亚晶界存在。

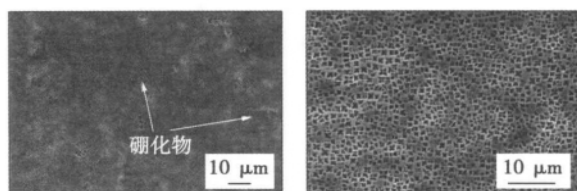


图8 TLP扩散焊接头微观组织形貌 图9 连接区微观组织形貌

Fig. 8 Microstructure of TLP diffusion bonding joint Fig. 9 Microstructure in bonding zone

采用在温度 $1\ 200\ ^\circ\text{C}$ 下保温9 h,然后在温度 $1\ 260\ ^\circ\text{C}$ 下保温2 h的TLP扩散焊工艺,接头在 $1\ 000\ ^\circ\text{C}$ 温度下进行了拉伸试验,接头平均抗拉强度为507 MPa。断口具有等轴韧窝特征,且在韧窝内有硼化物存在,如图10所示。结果表明,接头平均抗拉强度低于相同条件下基体的抗拉强度,且二者断口形貌明显不同,这说明接头断裂于连接区。在高温拉伸过程中,连接区脆性硼化物的存在使其成为断裂的敏感位置,在外力的作用下硼化物周围将产生应力集中,使硼化物与基体界面破碎而形成许多微小的孔洞,而后孔洞不断长大、聚集形成裂纹,裂纹在连接区萌生并沿连接区扩展直至断裂,从而形成具有韧窝特征的断口形貌。此外接头在温度 $1\ 000\ ^\circ\text{C}$ 、应力144 MPa下持久寿命可达到120 h以上。

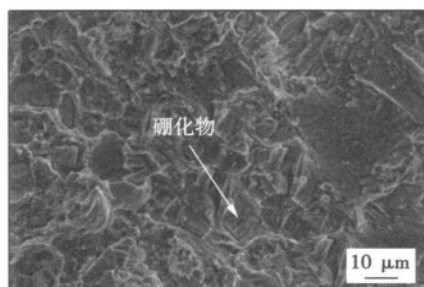


图10 TLP扩散焊接头高温拉伸断口形貌

Fig. 10 Morphology of joint fracture surface after tensile test under high temperature

3 结 论

(1) 接头由连接区和基体区所组成。连接区由等温凝固区和快速凝固区组成。等温凝固区主要由 γ 和 γ' 相组成,快速凝固区主要是由(Mo, W, Cr) B化合物和 γ 相共晶及花簇状的 γ 和 γ' 相共晶组织组成。

(2) 在温度 $1\ 000\ ^\circ\text{C}$ 下IC10单晶TLP扩散焊接头平均抗拉强度达到507 MPa,在温度 $1\ 000\ ^\circ\text{C}$ 、应力144 MPa下接头持久寿命可达到120 h以上。

(3) 接头高温拉伸断裂于连接区,断口具有等轴韧窝特征,且接头的断裂行为与连接区内的硼化物有关。

参考文献:

- [1] 侯金保,张 蕾,魏友辉. IC10合金TLP扩散焊接头组织与强度分析[J]. 焊接学报, 2008, 29(3): 89-92.
Hou Jinbao, Zhang Lei, Wei Youhui. Microstructure and strength analysis of IC10 alloy TLP-DB joint[J]. Transactions of the China Welding Institution, 2008, 29(3): 89-92.
- [2] 张 胜,侯金保,郭德伦,等. MGH956合金TLP连接机理及接头组织分析[J]. 焊接学报, 2004, 25(3): 43-47.
Zhang Sheng, Hou Jinbao, Guo Delun, et al. Transient liquid phase bonding mechanism and microstructure of MGH956 joints [J]. Transactions of the China Welding Institution, 2004, 25(3): 43-47.
- [3] 李晓红,毛 唯,郭万林,等. DD6单晶合金过渡液相扩散焊工艺[J]. 焊接学报, 2005, 26(4): 51-54.
Li Xiaohong, Mao Wei, Guo Wanlin, et al. Transient liquid phase diffusion bonding of a single crystal superalloy DD6 [J]. Transactions of the China Welding Institution, 2005, 26(4): 51-54.
- [4] Nishimoto K, Saida K, Kim D, et al. Transient liquid phase bonding of Ni-base single crystal superalloy CMSX-2 [J]. ISIJ International, 1995, 35(10): 1298-1306.
- [5] Kim D U, Nishimoto K. Bonding phenomena of transient liquid phase bonded joints of a Ni base single crystal superalloy [J]. Metals and Materials International, 2002, 8(4): 403-410.
- [6] Nishimoto K, Saida K, Kim D, et al. Bonding phenomena and joint properties of transient liquid phase bonding of Ni-base single crystal superalloys [J]. Welding Research Abroad, 1998, 44(11): 48-58.

作者简介: 郎 波,男,1980年出生,博士,高级工程师。主要从事扩散焊、摩擦焊的基础研究与工程应用工作。发表论文10余篇。
Email: langbo198009@163.com

was soaked in molten copper. It was found that the structure of oxide film changed after heating in low vacuum environment , and this film can not prevent the solution of stainless steel by the molten copper. Through investigation into the mechanism of removing oxide film on stainless steel sheet in vacuum condition and thermodynamic calculations , it was proposed that carbon could deoxygenate and weaken the oxide film. Once the molten copper met the stainless steel substrate by flowing through the cracked oxide film , the stainless steel would rapidly dissolve due to the diffusion of Ni atoms into the molten copper , and subsequently the oxide film would float on the molten copper. Finally , the oxide film would be removed under the action of surface tension in low vacuum condition.

Key words: brazing of stainless steel in low vacuum condition; mechanism of removing oxide film; carbon reductive; oxide film; solution

Optimizing of compressive stress region by local treatment technologies on Francis runner CHENG Guangfu¹ , WANG Huiting¹ , JI Shude² , FANG Hongyuan³ (1. State Key Laboratory of Hydro-power Equipment , Harbin Institute of Large Electrical Machinery , Harbin 150040 , China; 2. Institute of Astronautical Technology , Shenyang Institute of Astronautical Engineering , Shenyang 110034 , China; 3. State Key Laboratory of Advanced Welding and Joining , Harbin Institute of Technology , Harbin 150001 , China) . pp 97 – 100

Abstract: The existing of residual compressive stress increases the fatigue resistance of welding structures. The local compressive stress was realized around the fusion boundary in the Francis turbine runner by optimizing the welding process , where fracture could easily occur. And the influence of local heating and peening on the stress field in the fracture-easily-occurred region of runner was simulated and measured based on the real runner. The results indicate that the stress field in the fracture-easily-occurred region of runner can be regulated and controlled by local heating and peening processes. And the local compressive stress region was optimized. The value of residual compressive stress in the fracture-easily-occurred region of runner was further improved , and high compressive stress region was formed , especially , the compressive stress region was expanded. These processes can promote the realization of local compressive stress in the fracture-easily-occurred region of Francis runner and effectively enhance the fatigue resistance of the runner.

Key words: Francis runner; welding residual stress; local heating; peening; local compressive stress

Analysis on cooling flow field of electrode in plasma arc cutting torch CHEN Lihua¹ , WEI Jingyu² (1. Department of Mechanical Engineering , Changzhou Institute of Mechatronic Technology , Changzhou 213002 , China; 2. Hehai University Changzhou 213002 , China) . pp 101 – 104

Abstract: Two-dimensional numerical model for the cooling channel and electrode in plasma cutting torch was established with FLUENT commercial software , the relationship between the coolant flow field and geometry structure of the electrode was analyzed and the effects of four different electrode structures on the distribution of cooling flow field were investigated. For A-type electrode , there existed a zone where the flowing speed of the coolant was zero. For B-type electrode and C-type electrode , there was a back-flowing zone and zero-speed zone. For D-type

electrode , the arc transition in the cone-shaped electrode was beneficial to cooling of the electrode. Meanwhile , the effect of inserting depth of capillary tube on the cooling flow was simulated. When the ratio of inserting depth of capillary tube to the diameter of capillary tube was larger than 0.5 , there existed a zero-speed zone , however , when the ratio was around 0.2 , the distribution of fluid flow field was beneficial to cooling of the electrode.

Key words: inner structure of electrode; numerical simulation; flow field

Design and realization of fully digital intelligent pulse arc welding power source DUAN Bin , ZHANG Chenghui , SUN Tongjing , ZHANG Guangxian (School of Control Science and Engineering , Shandong University , Jinan 250061 , China) . pp 105 – 108

Abstract: Welding power supply system with high performance is the key to meet the requirement of pulse welding technology , which can generate accurate welding arc and high welding quality. First , the system design program was proposed for fully digital pulse inverter welding power supply , including the main circuit structure and hardware circuit of the control system , based on field programmable gate array and 32-bit micro-control unit. Second , the software design for the main control system was described using very high-speed integrated circuit hardware description language to realize the complex pulse welding technology sequence and steady arc control. Effective methods were investigated to improve the anti-interference capability and real-time performance of the system. Finally , the experiments were conducted , and the results showed that the designed fully digital intelligent pulse arc welding power source had high flexibility , robustness and reliability , which could satisfy rigorous demand of the welding arc so as to achieve satisfactory welding quality.

Key words: arc welding power source; field programmable gate array; hardware description language; anti-interference

Microstructure and mechanical properties of IC10 single crystal superalloy transient liquid phase diffusion bonding joint LANG Bo , HOU Jinbao , WU Song (Aero-Engine Technology Department , Beijing Aeronautical Manufacturing Technology Research Institute , Beijing 100024 , China) . pp 109 – 112

Abstract: Microstructural evolution of transient liquid phase (TLP) diffusion bonding joint of IC10 single crystal superalloy was investigated with scanning electron microscopy (SEM) and energy-dispersive spectrum (EDS) . The results show that the joint contained bonding zone and base material zone. The bonding zone consisted of isothermal solidification zone and rapid solidification zone. Rapid solidification zone could be eliminated by increasing welding time. The size of γ' phase in the base material reached 0.9 μm when the welding time increased from 2 h to 8 h. The mechanical properties of the joints can be effectively improved by restraining formation of grain boundary in TLP diffusion bonding joint and postweld solution treatment. The average tensile strength of the joints was 507 MPa at 1 000 $^{\circ}\text{C}$. The creep rupture life of the joints reached 120 h under the condition of 144 MPa stress at 1 000 $^{\circ}\text{C}$.

Key words: IC10 single crystal superalloy; TLP diffusion bonding; microstructure